Available online at www.sciencedirect.com
ScienceDirect
Journal of Sound and Vibration 318 (2008) 868–883
JOURNAL OF SOUND AND VIBRATION
www.elsevier.com/locate/jsvi

Finite element modelling of low-speed femur reaming using reamers with irregular tooth spacing

S. Towfighian[a], K. Behdinan[a,*], M. Papini[b], Z. Saghir[b], P. Zalzal[c], J. de Beer[c]

[a]*Department of Aerospace Engineering, Ryerson University, Toronto, Ontario, Canada M5B 2K3*
[b]*Department of Mechanical and Industrial Engineering, Ryerson University, Toronto, Ontario, Canada M5B 2K3*
[c]*Orthopedic Surgery Division, McMaster University, Hamilton, Ontario, Canada*

Received 3 October 2006; received in revised form 17 April 2008; accepted 21 April 2008
Handling Editor: S. Bolton
Available online 24 June 2008

Abstract

Reaming of the cancellous bone of the femur is performed in certain orthopaedic procedures, in order to accommodate insertion of implants such as intramedullary nails. In such processes, the reamers spin at a maximum of 250 rev/min resulting in low-frequency vibrations, which can result in the formation of multicornered holes or non-cylindrical holes. These non-cylindrical holes can lead to improper fixation, which increases healing duration. Simulation of low-speed reaming in the femur analogue was conducted by using a finite element model of the reamer with two different models for reamer blade loads: concentrated forces on the tool tip and distributed forces on the engagement length of the reamer. The model of the process is quasi-static in a characteristic form. The specific cutting pressure, an important parameter in the governing equation, was found experimentally for this purpose. The effects of reaming condition, reamer size, and irregular tooth spacing on stability were investigated. An optimum irregular tooth spacing for a common six-flute reamer, resulting in the most stable reaming process was proposed. Hole profiles and tool axis trajectory of the tool were simulated for both regular and optimum irregular tooth spacing cases. The improvements in the hole quality from using the proposed irregular tooth spacing; benefits of which include expedition of post-operative healing, were demonstrated through simulated three-dimensional hole profiles.

1. Introduction

Intramedullary nailing is a modern surgical method of internal fracture fixation used in long bones such as the femur. The nails' function is to stabilize the fracture fragments, allowing load transfer across the fracture site while maintaining anatomical alignment of the bone [1]. In order to prepare the distal femoral canal for intramedullary nails, straight reamers are used to remove the cancellous bone. Axial and torsional reamer cutting loads measured during the reaming process are highly vibratory, indicative of tool lateral vibration during the process. Vibratory movement of the reamer in the femoral canal can lead to an oversized and lobed canal [2], which directly affects the selection of the final nail size in the clinical procedure. Nails with larger

*Corresponding author. Tel.: +1 416 979 5000x6414; fax: +416 979 5265.
E-mail address: kbehdina@ryerson.ca (K. Behdinan).

0022-460X/$ - see front matter © 2008 Elsevier Ltd. All rights reserved.
doi:10.1016/j.jsv.2008.04.043

Nomenclature

The definition of symbols is done in alphabetical order:

d	diameter of the reamer (mm)
f, feed	feed (mm/rev)
F_{ci}	cutting force on the ith tooth (N)
F_{ri}	rubbing force on the ith tooth (N)
F_x	applied force on the reamer in the x-direction (N)
F_y	applied force on the reamer in the y direction (N)
H_{nominal}	feed per tooth (mm/rev)
I	principal moment of inertia of the reamer area about x- or y-axis (mm^4)
k_r	rubbing coefficient or stiffness (N/mm)
k_s	specific cutting pressure (N/mm^2)
L_0	length of the reamer (mm)
N	number of teeth
R_{nominal}	width of cut (mm)
t	time (s)
$x(t)$	tool center displacement in the x direction (mm)
$y(t)$	tool centre displacement in the y direction (mm)

Greek symbols

α	cutting angle (rad)
θ_r	angular width of radial margin (rad)
ϕ_I	angle between the x-axis and the line from centre to the flute of ith tooth (rad)
Ω	spindle speed (rev/min)

diameters often cause thermal damage to the bone and, in open fractures, can result in an increased infection rate by the disruption to the tenuous remaining blood supply of the femur [3,4]. Consequently, lobed canals require a longer healing process than a smooth intramedullary canal. Therefore, a reduction in the vibration during reaming would be beneficial for the expedition of the healing process after femur surgeries or similar surgeries on the tibia or humerus.

Vibratory excitation of the fracture fragments is also a potential factor affecting intravazation [2]. The risk of a bone marrow fat embolism caused by intramedullary reaming has been recognized as a possible complication. Bone marrow fat embolized to the intravascular component causes lung contusion which, in combination with thoracic trauma and a femoral shaft fracture, may lead to postoperative problems with pulmonary dysfunction [5].

In the past, studies on dynamics and vibration during reaming were mostly conducted for machining of metals. Very little work has been done to simulate the process in bone tissue. An experimental study on the mechanical loads applied on the reamer exists [3], but it did not consider the dynamics and vibrations of the reamer. Peindl et al. [3] evaluated the mechanical loading experienced by four clinically used intramedullary reamer cutter designs to evaluate the effects of variation in speed and feed rate on reamer system performance. All systems demonstrated reduced maximal loads/torques for small reamer sizes at drilling speeds (750 rev/min), rather than reaming speeds (250 rev/min). Individual systems demonstrated measurable differences in sensitivity to alterations in operating speed, indicating that some designs are not amenable to operation at increased speeds. These tests demonstrate that appropriate control of reaming speeds (rev/min) can be used to minimize mechanical loading for all systems.

The main objective of the present work was to model the reaming process in bone, so that the dynamics and vibration of reamers used in orthpaedic procedures could be investigated. To this end, a finite element model developed for low-speed reaming in aluminium [6], which utilizes a new model for applying the reamer forces, was employed. In Ref. [6], forces on the reamer were applied as uniform distributed forces on the engagement length of the reamer, and the reamer axis trajectory and resulting hole profiles were simulated, for the reaming of aluminium. The present work utilizes this model, together with the experimental cutting forces acquired by Hojabr [7] for an artificial bone analogue, to characterize the vibration in orthopaedic reaming procedures. The vibration characteristics are presented, as well as the simulated bone canal profiles.

A secondary objective of the present work was to investigate methods to reduce the vibration in the bone during the reaming process, in order to expedite healing after surgery. The model was used to investigate a variety of reamer designs to maximize the canal circularity and stability during reaming, thereby leading to smoother canals after the reaming process. This improvement was done by designing a reamer with an

irregular pitch, based on previously reported results that claim a positive effect of irregular tooth spacing on improving hole circularity after machining [8,9].

2. Experimental set-up

Reaming in the laboratory was done on an artificial bone analogue that was designed to match the material properties of the human femur [7]. The analogue consists of a two concentric tubes, the inner one representing cancellous bone and the intramedullary canal, and the other tubular shell representing cortical bone. A schematic cross-section of the femur analogue is shown in Fig. 1. The inner tube representing the cancellous bone, was made from an open-cell porous carbon foam (Touchstone Research Laboratory, Triadelphia, WV, USA), having a density of 270 kg/m^3, modulus of elasticity of 550 MPa, and strength of 6.2 MPa [10]. It was 350 mm long, with inner and outer diameters of 10 and 15 mm, respectively. The outside layer, representing the cortical bone, was made of an open-cell porous plastic foam (Porex Porous Products Group, Fairburn, GA, USA), and was 350 mm long, with inner and outer diameters of 15 and 32 mm, respectively.

In the experiments of Ref [7], the simulated intramedullary canal was filled with the Vaseline/paraffin wax mixture representing bone marrow, and initially reamed using a 10 mm diameter reamer (Stryker Howmedica Corp., Kalamazoo, MI, USA). The experimental set-up and the reamer used for performing the reaming tests by Hojabr [7] is shown in Figs. 2 and 3, respectively. The simulated bone was re-reamed repeatedly with reamer bit diameters increasing in 0.5 mm increments, up to a maximum diameter of 15 mm. The reaming process included forward reaming for 23.5 cm and backward reaming for the same length. Feed rate was kept constant for each reamer size by using a computer controlled feed table to keep the spindle speed and advancement speed constant. The multiaxis load cell shown in Fig. 2 was used by Hojabr [7] to measure the applied cutting forces F_x and F_y, which will be used for the analysis in Section 4. These forces are available for the reaming process conditions that are listed in Table 1. Data for reamer sizes up to 14 mm was selected because the presence of cancellous bone analogue, as in real femur surgeries, was guaranteed.

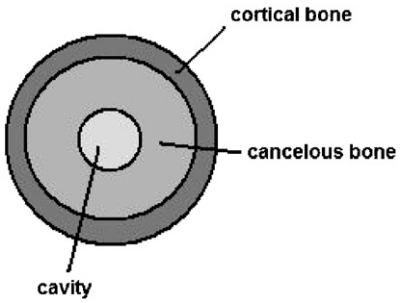

Fig. 1. Schematic cross-section of the femur.

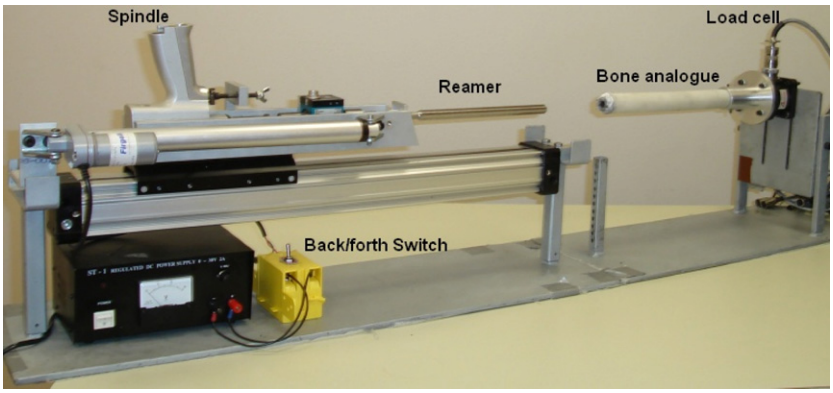

Fig. 2. Reaming experiment set-up.

Fig. 3. Reamer (Stryker Howmedica Corp., Kalamazoo, MI, USA).

Table 1
The reaming process parameters for measuring cutting forces

Reamer size (mm)	Spindle speed, Ω (rev/min)	Advancement speed, s (mm/s)	Feed $= 60s/\Omega$ (mm/rev)
12,12.5,13,13.5,14	50,200	10,50	3–60

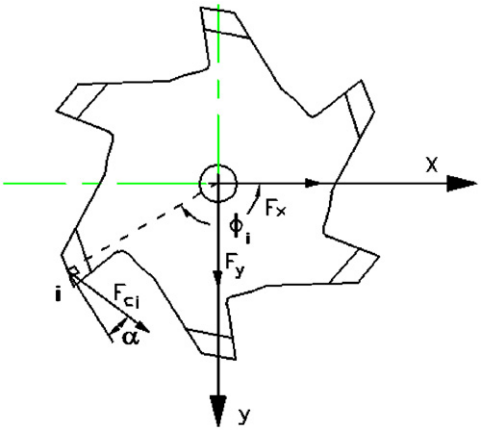

Fig. 4. Cutting and rubbing forces analysis.

3. Force analysis

The load cell in the reaming experiments of Ref. [7] measured the reactive forces in the directions shown in Fig. 4 at the centre of the bone model, which is aligned axially with the centre of the six-flute reamer.

These reactive forces result from the vector summation on the reamer teeth. An analysis is needed to decompose these forces into their components on the reamer teeth (Fig. 4), and consequently relate them to the required coefficients. This analysis is performed as follows.

F_x and F_y, which are measured during the reaming experiments at the tool centre, are the summation of cutting and rubbing force components on the reamer teeth in the x and y directions. Rubbing forces, F_{ri} are caused by teeth rubbing against the newly cut material. The rubbing force, known as process damping by researchers [11–13], depends not only on the interference between the newly cut material and the clearance face of the workpiece, but also on the coefficient of friction between the two materials. As can be seen in the equation for rubbing forces developed by Bayly [13], increasing the coefficient of friction increases α_μ, which leads to greater rubbing forces. It should be noted that because of the presence of Vaseline/paraffin mixture, the coefficient of friction between the carbon foam and the stainless steel is much less than the one between the aluminium and stainless steel. Therefore, the rubbing force has been assumed to be negligible in this application due to a very low friction force. F_x and F_x then can be expressed in terms of cutting forces on the teeth as

$$F_x = \sum_{i=1}^{6} F_{ci} \cos \theta_i \tag{1}$$

and

$$F_y = \sum_{i=1}^{6} F_{ci} \sin \theta_i, \tag{2}$$

where

$$\theta_i = \phi_i - \alpha - \frac{\pi}{2} \quad (i = 1, 2, ..., 6) \tag{3}$$

and F_{ci}, $i = 1,\ldots,6$ are the cutting forces on the ith tooth (i is numbered clockwise from the x-axis), and α is the cutting angle, which is assumed constant at a value of $\pi/6$ for six-flute reamers with zero rake angles [14,15]. ϕ_i is the angle between the line from the tool centre to the ith tooth flute and the x-axis (Fig. 4).

Based on geometry and the definition of cutting forces introduced by Bayly et al. [13], a method has been developed in Ref. [16] to find the derivatives of F_x, F_y with respect to feed:

$$\frac{dF_x}{dfeed} = m = c_1 k_s \cos \theta_2, \tag{4}$$

$$\frac{dF_y}{dfeed} = n = c_1 k_s \sin \theta_2, \tag{5}$$

where

$$c_1 = 4\frac{R_{\text{nominal}}}{N}, \tag{6}$$

where k_s is the specific cutting pressure, R_{nominal} is the width of cut, θ_2 is determined from Eq. (3) and is a function of the second tooth angle, and N is the number of teeth. By plotting F_x, F_y versus feed, one can obtain the slopes m and n, respectively. Equating k_s in two Eqs. (4) and (5), leads to

$$\frac{m}{c_1 \cos \theta_2} = \frac{n}{c_1 \sin \theta_2}. \tag{7}$$

Rearranging Eq. (7) yields

$$\theta_2 = \text{arc tan}\left(\frac{n}{m}\right). \tag{8}$$

Substituting Eq. (8) into Eq. (5), the final relation of specific cutting pressure, k_s is found as

$$k_s = \frac{n}{c_1 \sin\left(\text{arc tan}(n/m)\right)}. \tag{9}$$

4. Cutting pressure coefficient of the femur analogue

The specific cutting pressure of the bone analogue, k_s, can be obtained from the forces measured in the centre of the tool, based on the theoretical analysis of the previous section. Some primary data analysis must be performed on the raw data from the experiments in order to determine this coefficient.

Fig. 5 shows the forces profile created from data measured by Hojabr [7], for reaming of the bone analogue with a 13.5 mm reamer, for the different reaming conditions listed in Table 1. Force profiles for other sizes of the reamer for the same reaming conditions can be found in Ref. [7]. The reamer begins rotating at a distance of approximately 100 mm from the end of the bone analogue. It then advances 235 mm into the bone analogue, before reaming back over the same length, and returning to its original position. In Fig. 5, the first steep change in the forces shows the moment when the reamer touches the bone analogue, and the last steep change shows the moment when the reamer exits the bone analogue. The peak point in the forces shows the approximate moment when the reamer starts reaming back. The gradual increase in the force magnitude for one way reaming is because of the increasing bone marrow pressure inside the femur analogue. The pressure of

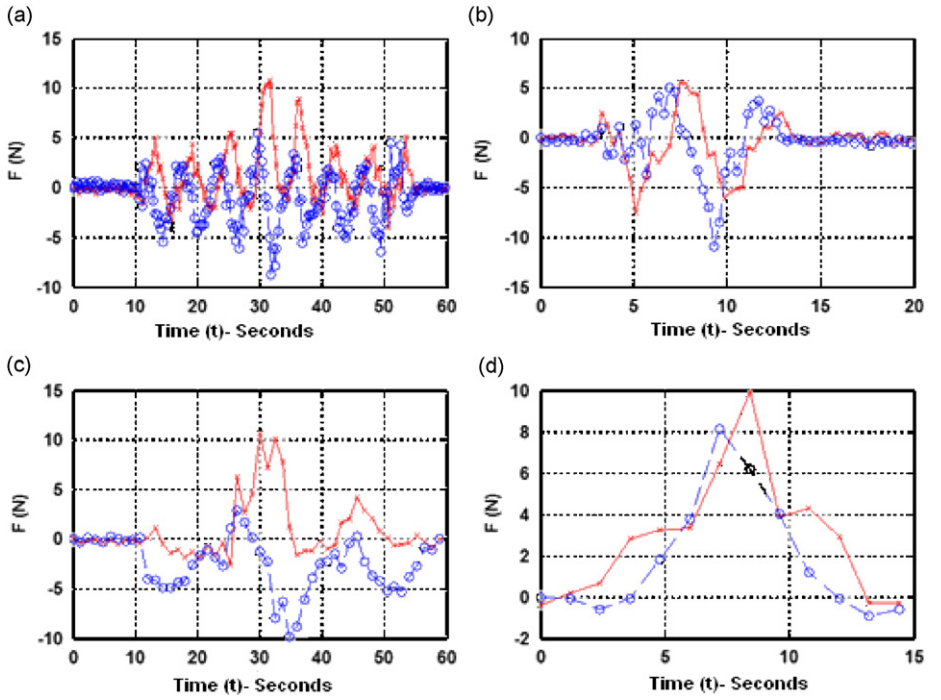

Fig. 5. Forces profile at the centre of the reamer during reaming experiment [7] for 13.5 mm diameter reamer (a) $\Omega = 200$ rev/min, $s = 10$ mm/s, (b) $\Omega = 200$ rev/min, $s = 50$ mm/s, (c) $\Omega = 50$ rev/min, $s = 10$ mm/s (d) $\Omega = 50$ rev/min, $s = 50$ mm/s. —×— F_x —○— F_y.

the synthetic marrow mixture, which is present inside the cancellous bone is minimum at the free end of the bone analogue, and it is maximum at the fixed end of the bone analogue [7]. A similar trend therefore is seen for force profile in Fig. 5.

Reamer forces applied for the analysis were considered from the moment when reaming began to its maximum penetration, i.e. 235 mm in length. Using a time step of one revolution period of the reamer, the associated forces were extracted from the data and the averages calculated. In this manner, for each of the profiles in Fig. 5, one point is found in the graphs of F_x and F_y versus feed depicted in Figs. 6 and 7, respectively. In these figures, feed rate 3 mm/rev corresponds to $\Omega = 200$ rev/min and $s = 10$ mm/s, feed rate 12 mm/rev corresponds to $\Omega = 50$ rev/min and $s = 10$ mm/s, feed rate 15 mm/rev corresponds to $\Omega = 200$ rev/min and $s = 50$ mm/s, and feed rate 60 mm/rev corresponds to $\Omega = 50$ rev/min and $s = 50$ mm/s. The forces versus feed relationships are strongly dependent on the changes of the bone marrow pressure inside the cancellous bone analogue. Increasing the advancement speed and decreasing the spindle speed results in higher feed (feed $= 60s/\Omega$), higher overall pressure in the bone marrow [7] and consequently higher total forces on the reamer. For different reamer sizes except the 13 mm diameter reamer, resultant total forces from these graphs increase with decreasing of spindle speed and increasing of advancement speed. The drop which is seen in the graphs at feed of 15 mm/rev shows that the spindle speed effect on pressure and forces is more than the advancement speed effect.

According to Eqs. (4) and (5), the slopes of the best fit line on graphs of F_x, F_y versus feed, yield m and n, respectively, and by substituting these values into Eq. (9), the specific cutting pressure, k_s, can be obtained. Best fit m and n coefficients for all reamer sizes are listed in Table 2, together with the corresponding R^2 values. From the R^2 of the fitted lines in Table 2, it can be inferred that the lines for F_x and F_y versus feed, on average, explain 79% and 56%, respectively, of the total variation about the average.

To determine the specific cutting pressure k_s, first c_1 was found from Eq. (6) by substituting the number of teeth $N = 6$ and width of cut in the experiments $R_{\text{nominal}} = 0.5$ mm. Substitution of this c_1 value with the

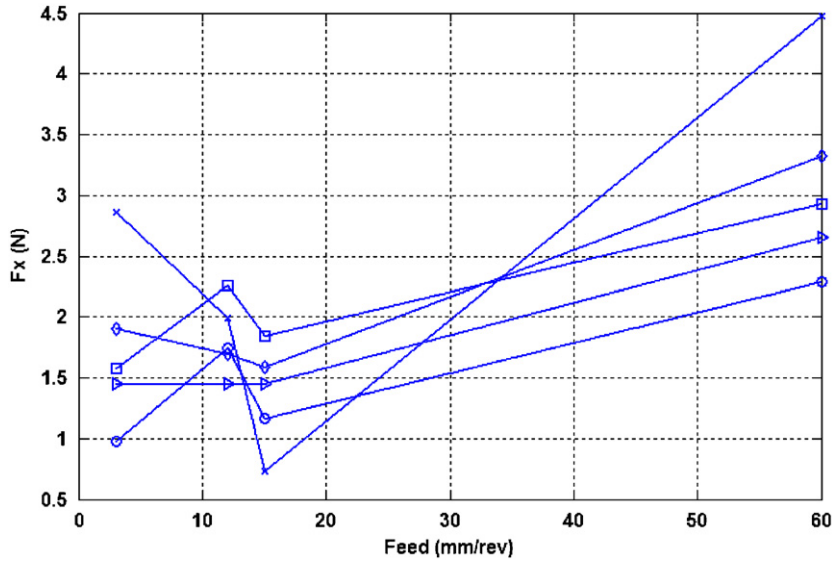

Fig. 6. F_x versus feed for different sizes of the reamer. $D = 12$ mm, $D = 12.5$ mm, $D = 13$ mm $D = 13.5$ mm 14 mm.

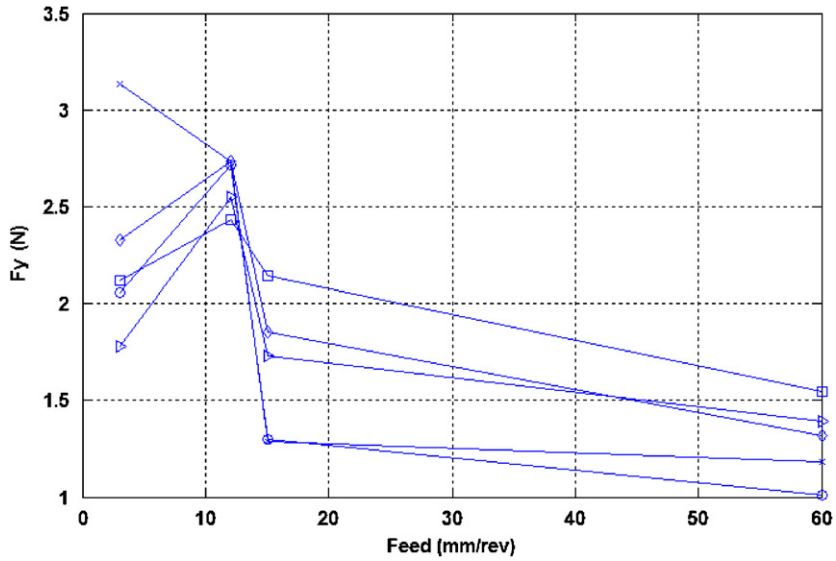

Fig. 7. F_y versus feed for different sizes of the reamer. $D = 12$ mm, $D = 12.5$ mm, $D = 13$ mm $D = 13.5$ mm 14 mm.

Table 2
Statistical and line fitting slope results of F_y versus feed graphs

Reamer diameter (mm)	M (N rev/mm)	R^2	n (N rev/mm)	R^2
12	0.0202	0.757	−0.0208	0.473
12.5	0.0212	0.851	−0.0129	0.771
13	0.0438	0.504	−0.0283	0.525
13.5	0.0295	0.876	−0.0197	0.681
14	0.0231	0.961	−0.0114	0.354
Avg	0.0276	0.790	−0.0186	0.561

average of m and n from Table 2 into Eq. (9) yields the specific cutting pressure

$$k_s = \frac{-0.0186}{1/3\ \sin\left(\text{Arc tan}(-0.0186/0.0276)\right)} = 0.1\,\text{N/mm}^2. \tag{10}$$

This value is the specific cutting pressure of the stainless steel reamer on the carbon foam, which is representative of cancellous bone analogue.

5. Finite element modelling of reaming in the femur analogue

In order to study the deformation of the reamer caused by cutting and rubbing forces, the reamer is divided lengthwise into a number of elements based on the Euler–Bernoulli beam model. Finite element modelling of the reaming in the bone model was performed in a similar manner as that used for reaming of aluminium in Ref. [6], which considered the effect of flexibility of the reamer on the vibrations. The forces on the reamer were assumed to be in two scenarios: concentrated at the tip, and uniformly distributed on its variable engagement length. In a real reaming process, because the reamers are tapered with small angles, the engagement length of the reamer and the workpiece increases with reamer advancement, and the loads are not limited to the tool tip. In the model developed, the applied forces are assumed uniformly distributed on this length. For more accurate results and hole profile simulations, the distributed force model is employed, but for initial evaluation of different parameters, the concentrated force model is used here (Sections 5.2.1 and 5.2.2).

The specifications of the reamer and the reaming process used in the finite element modelling are listed in Table 3. After developing the finite element model of the reamer, the movement of the tool axis was determined by solving the characteristic form of the equilibrium equations for eigenvalue and eigenvector parameters a, b, c, and d, as described in Ref. [6], which was based on the quasi-static model proposed by Bayly [13].

Finally, the axis tool vibration for each mode was determined by [13]

$$\vec{x} = \begin{bmatrix} x(t) \\ y(t) \end{bmatrix} = A\mathrm{e}^{at} \begin{bmatrix} c\cos bt & -d\sin bt \\ \cos bt & \end{bmatrix} \tag{11}$$

where a gives the decaying or growing rate of vibration, b is the frequency of the oscillation and c and d are coefficients of the amplitude A, which depends on the initial conditions. All the results presented from this point forward, are developed for the reamer with a 13 mm diameter.

Table 3
Experimental reaming specifications[a]

Symbol	Description	Value
N	Number of teeth	6
D	Diameter of the reamer	13 mm
L_0	Length of the reamer	235 mm
Ω	Spindle speed	50, 200 rev/min
S	Advancement speed	10, 50 mm/s
F	Feed	3–60 mm/rev
R_{nominal}	Width of cut	0.5 mm
H_{nominal}	Feed per tooth	0.5–10 mm/rev
k_s	Specific cutting pressure	0.1 N/mm^2
k_c	Cutting stiffness ($k_c = k_s(R_{\text{nominal}} + H_{\text{nominal}})$	0.1–1.05 N/mm^2
K_r	Rubbing stiffness	0 N/mm^2
K	Reamer bending stiffness for one element model, $k = 3EI/L_0^3$	34.6 N/mm
α	Cutting angle	$\pi/6$
θ_r	Angular width of radial margin	0

[a]Reamer material is stainless steel 17–4 pH and the material that is being reamed is carbon foam.

Table 4
Decay rate for regular tooth spacing

Pitch angle (deg)	Mode 1 ($b = 1$)	Mode 2 ($b = 5$)	Mode 3 ($b = 7$)	Mode 4 ($b = 11$)
$\phi = [0\ 60\ 120\ 180\ 240\ 300]$	−0.190	−0.190	−0.190	−0.190

Table 5
Decay rate for irregular tooth spacing [55 65 50 70 45 75] yielding the minimum values for different modes

Pitch angle (deg)	Min for mode	Mode 1 ($b = 1$)	Mode 2 ($b = 5$)	Mode 3 ($b = 7$)	Mode 4 ($b = 11$)	Average (1–3)
$\phi = [0\ 70\ 145\ 210\ 255\ 310]$	1	−0.190	−0.783	−0.898	−1.28	−0.624
$\phi = [0\ 45\ 95\ 160\ 235\ 305]$	2, 1–3	−0.190	−0.811	−1.03	−1.06	−0.677
$\phi = [0\ 65\ 140\ 210\ 260\ 305]$	3	−0.190	−0.524	−1.07	−1.05	−0.596
$\phi = [0\ 50\ 95\ 170\ 235\ 305]$	4	−0.190	−0.680	−0.724	−2.09	−0.531

5.1. Regular and irregular spacing of reamer teeth

A similar approach of using irregular pitch spacing for optimal reaming in aluminium [6,16] was used in the present work for reaming of the bone analogue. Using the data listed in Table 3, building the finite element model of the reamer, and solving the equilibrium equations, the tool axis movement is determined by eigenvalues and eigenvectors results, as in Eq. (11). It is noted that stability during reaming depends on a in Eq. (11), with a negative value showing a decaying vibration and a positive value showing growing vibration.

For a comparison of stability during reaming for a reamer with regular pitch spacing and different irregular spacing, the decay rate a was obtained as listed in Tables 4 and 5. In Table 5, the irregular spacing of reamer teeth was considered for a minimum deviation of 5° and maximum deviation of 15° from regular spacing with 5° increments or decrements. The finite element model of the reamer had 32 elements lengthwise, and utilized the uniform distributed force model. The real part of the eigenvalue for the distributed force model is time sensitive (Fig. 12), and was calculated at the end of the reaming time, when the lowest magnitude rate of decay occurs. This reaming condition is the most severe for a feed of 60 mm/rev, as explained in Section 5.2.1.

For an irregularly spaced group of teeth [55,65,50,70,45,75], in the range specified above, the power of the exponential term in Eq. (11), a, was calculated for 720 possible orientations of teeth, and those that yielded the minimum decay rate for each mode and the minimum average for the first three modes, are listed in rows of Table 5. In addition, the frequency of oscillation, b in cycles/rev, is also found in Tables 4 and 5.

Comparing Table 4 for regular and Table 5 for irregular spacing, it can be seen that regular tooth spacing for reaming in the bone analogue itself produced a damped vibration, but irregular spacing improves the stability due to the more rapid exponential decay rate of the vibration amplitude (i.e. more negative decay rates). In Table 5, the second spacing for the teeth yields the highest average of decay rate magnitude for the first three modes. Therefore, for further analysis, this set of angles [0 45 95 160 235 305] was chosen for irregular spacing, as depicted in Fig. 8. This irregular tooth spacing is the same as that found by Towfighian et al. [6] for the most stable reaming process in aluminium. The proposed optimum irregular tooth spacing for reaming of the femur analogue, therefore, may also be the optimum for other applications.

5.2. Stability analysis

Using the finite element model of the process developed in Ref. [6], based on the quasi-static model of Bayly et al.[13], the tool axis motion was determined by using Eq. (11). The power of the exponential term in the equation, a, is the main criteria for stability analysis, as it determines at which rate the vibrations are damping or growing. In this section, the effects of reaming conditions and reamer size on stability are first investigated, for the one element model of the reamer with the concentrated force at the tip. Then, a stability analysis will be

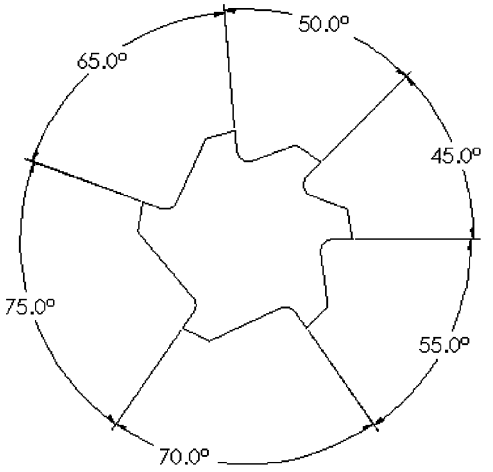

Fig. 8. Irregular tooth spacing for reaming in the femur analogue.

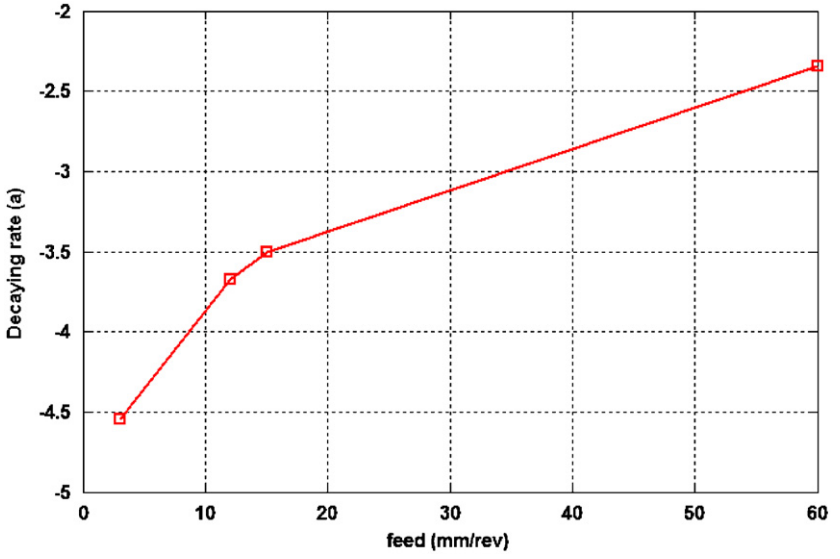

Fig. 9. Decaying rate, a, versus feed.

conducted for the reamer with regular and irregular spacing, and the two force models (i.e. concentrated and uniform distributed).

5.2.1. Reaming condition effect

In order to find the worst reaming process condition for stability during the process that is used for the simulations, the changes of decay rate, *a* versus feed are depicted in Fig. 9 for the one element model of the reamer with concentrated force at the tip. As the reamers have regular spacing, decay rates shown here are the same for all modes of vibration for the reaming specification given in Table 3. Fig. 9 shows that the decay rate becomes closer to zero as the feed increases; i.e. the stability becomes weaker by increasing the feed rate. Therefore, the worst condition is for the highest feed, 60 mm/rev, which can be reached at a speed of 50 mm/s and 50 rev/min. From this point forward, all the results are obtained for this most severe condition.

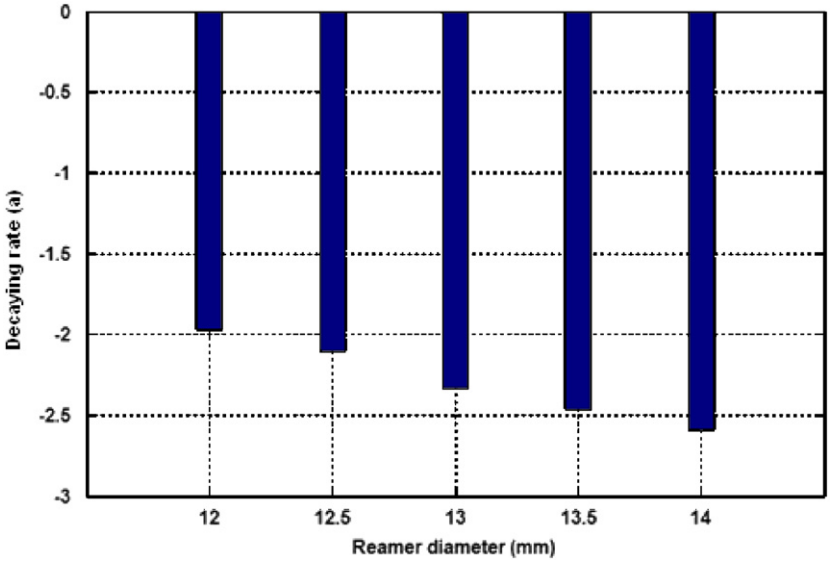

Fig. 10. Decaying rate, a, for different reamer sizes.

Table 6
Principal moment of inertia about the x-axis for reamers with different diameters, d

	$d = 12$ mm	$d = 12.5$ mm	$d = 13$ mm	$d = 13.5$ mm	$d = 14$ mm
Principal moment of inertia about the x-axis, I (mm^4)	525.23	607.79	788.42	910.87	1043.17

5.2.2. *Reamer size effect*

The effect of the size of the reamer on the decay rate is shown in Fig. 10. In this figure, the decay rate is depicted for different reamer sizes with the same length ($L_0 = 235$ mm) and material for the one element reamer, with the concentrated force at the tip. As the reamers have regular spacing, decay rates shown here are the same for all modes of vibration for the reaming specification of Table 3. It is evident that reaming with larger diameter reamers is more stable because the reamers have higher principal moments of inertia (Table 6), which result in higher bending stiffness. Therefore, increasing the bending stiffness by using reamers with a higher modulus of elasticity, shorter length and larger diameter will result in higher stability.

5.2.3. *Applied force model effect*

The first scenario considered was the concentrated force model on the one element model of the reamer. Using the data from Table 3 for reaming in the bone analogue, a, b, c, and d in Eq. (11) were obtained for regular and irregular tooth spacing. The frequency of oscillation, b in cycles/rev and the parameters c and d are listed in Table 7, and a is listed in Table 8.

From Table 8, it can be seen that irregular spacing changes the frequency of vibration for modes 2–4 and the parameter c in all modes, but parameter d remains unchanged. This implies that irregular spacing changes the characteristic of the vibration, and the most important effect can be noticed in Table 8, where it can be seen that irregular spacing gives higher decay rate magnitudes for modes 2–4, although it has almost the same decay rate as regular spacing for the first mode of vibration. Therefore, an improvement in stability with irregular spacing is evident for higher modes.

For the second scenario considered; i.e. a reamer with a different number of elements lengthwise and with the distributed force model, results for decay rate, a versus time for the case of even spacing, are shown in Fig. 11 for the first four modes, which are coincident. For reamer models with a large number of elements, the

Table 7
Frequency value b and parameters c and d (backward; $d=-1$, forward; $d=1$)

	Mode 1	Mode 2	Mode 3	Mode 4
Regular spacing				
Frequency, b (cyc/rev)	2	4	8	10
Parameter d	Backward	Forward	Backward	Forward
Parameter c	−0.008	−0.008	−0.008	−0.008
Irregular spacing				
Frequency, b (cyc/rev)	2	3.6	7	8.5
Parameter, d	Backward	Forward	Backward	Forward
Parameter, c	0.0209	−0.1104	0.7666	−1.0881

Table 8
Real part of the eigenvalue, a for different modes for regular and irregular spacing

Regular spacing			
Mode 1	Mode 2	Mode 3	Mode 4
−2.3350	−2.3350	−2.3350	−2.3350
Irregular spacing			
Mode 1	Mode 2	Mode 3	Mode 4
−2.3410	−2.5438	−2.7670	−2.7816

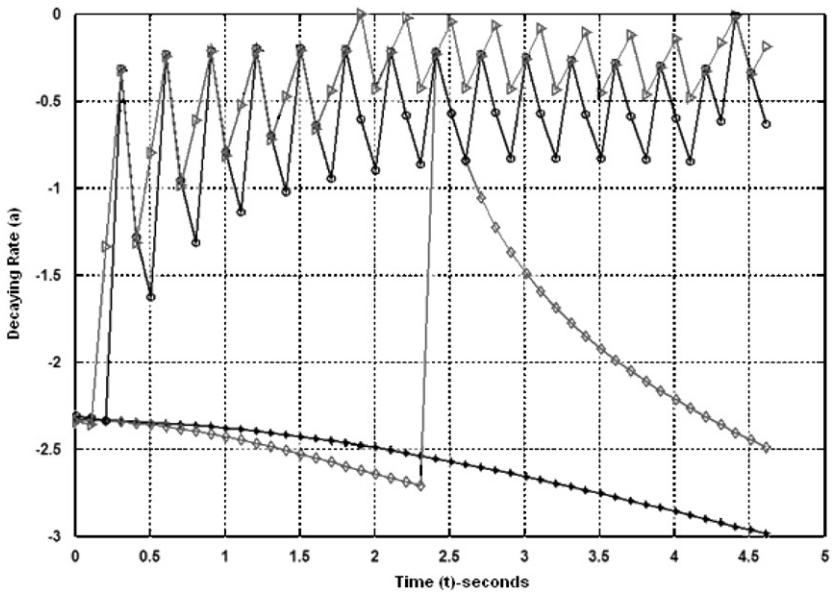

Fig. 11. Vibration decaying rate, a, versus time for the reamer with even tooth spacing and the distributed force model for the first to fourth modes. ——+——. 1 element ——◇——; 2 elements; ——○—— 16 element; ——▷—— 32 elements.

first mode of vibration for both regular and irregular tooth spacing changes from a damped vibration to almost a periodic vibration over time. In Fig. 11, the decay rate magnitude decreases with increasing number of elements and also with the passage of time. In addition, increasing the number of elements leads to a convergence of the results, as can be seen in the results of 16- and 32-element models, which are much closer than the results for one- and two-element models. For models of more than 32 elements, the results did not change significantly, indicating finite element model convergence.

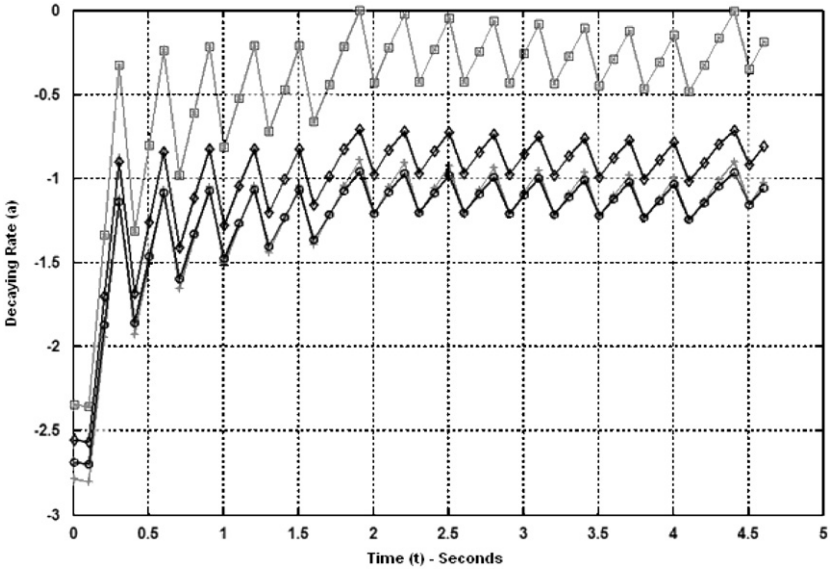

Fig. 12. Vibration decaying rate, a, versus time for the reamer with even and uneven tooth spacing, 32 element lengthwise and the distributed force model for the first four modes.–□– All modes, regular spacing; —×— mode1, irregular spacing; —◇— mode2, irregular spacing —+— mode3, irregular spacing; —○— mode4 irregular spacing.

In Fig. 12, results for decay rate versus time for both even and uneven spacing for the 32 element model are presented. Results for all modes for regular spacing are coincident, but for irregular spacing they are distinctive. It can clearly be seen that the decay rate for the first mode of vibration is coincident both for regular and irregular spacing cases, but irregular spacing results in a significantly higher damping rate magnitudes for the second to fourth modes. The irregular spacing thus improves the stability during the reaming process, and results in a smoother hole texture (Section 5.3X). Decreasing of the damping rate over time is also noticeable in this figure.

5.3. 2D and 3D hole profiles

Reamer-axis trajectory and the trace of the tip are shown in Fig. 13 for regular and irregular spacing, for the 13 mm diameter reamer case. The reamer is in contact with the bone analogue, and thus the trace of the tool tip also gives the two-dimensional (2D) hole profile. The decreasing tool axis vibration effect of irregular spacing on modes 2–4 is obvious when parts of a and b of Figs. 5–6 are compared.

Although reaming in the bone analogue is a damped vibration by having a negative value for the power of the exponential term, changes of damping rate during the process, as depicted in Fig. 12, cause variation of the hole radius along the depth of the hole. This can be seen in the simulated three-dimensional (3D) hole profile presented in Fig. 14, in which the z-axis is the time in seconds and x and y axes are the hole axes in mm. As shown in Fig. 14, this non-uniformity along the depth of the hole vanishes by employing the irregular tooth spaced reamer. Improving the smoothness of the hole wall is more obvious in the vibration of modes 2–4, consistent with the discussions in Section 5.2.

In a real surgical application, all vibration modes can be present in combination. Improving the resulting hole profile smoothness for individual modes as much as possible, as investigated here will facilitate the healing process. Another way of improving hole smoothness is by using a reamer material with a higher modulus of elasticity and using shorter reamers with larger diameters, as discussed in Section 5.2.

6. Conclusions

Simulation of the low-speed reaming in the femur analogue was conducted by using the finite element method. Finite element discretization was performed for the cantilevered reamer model based on

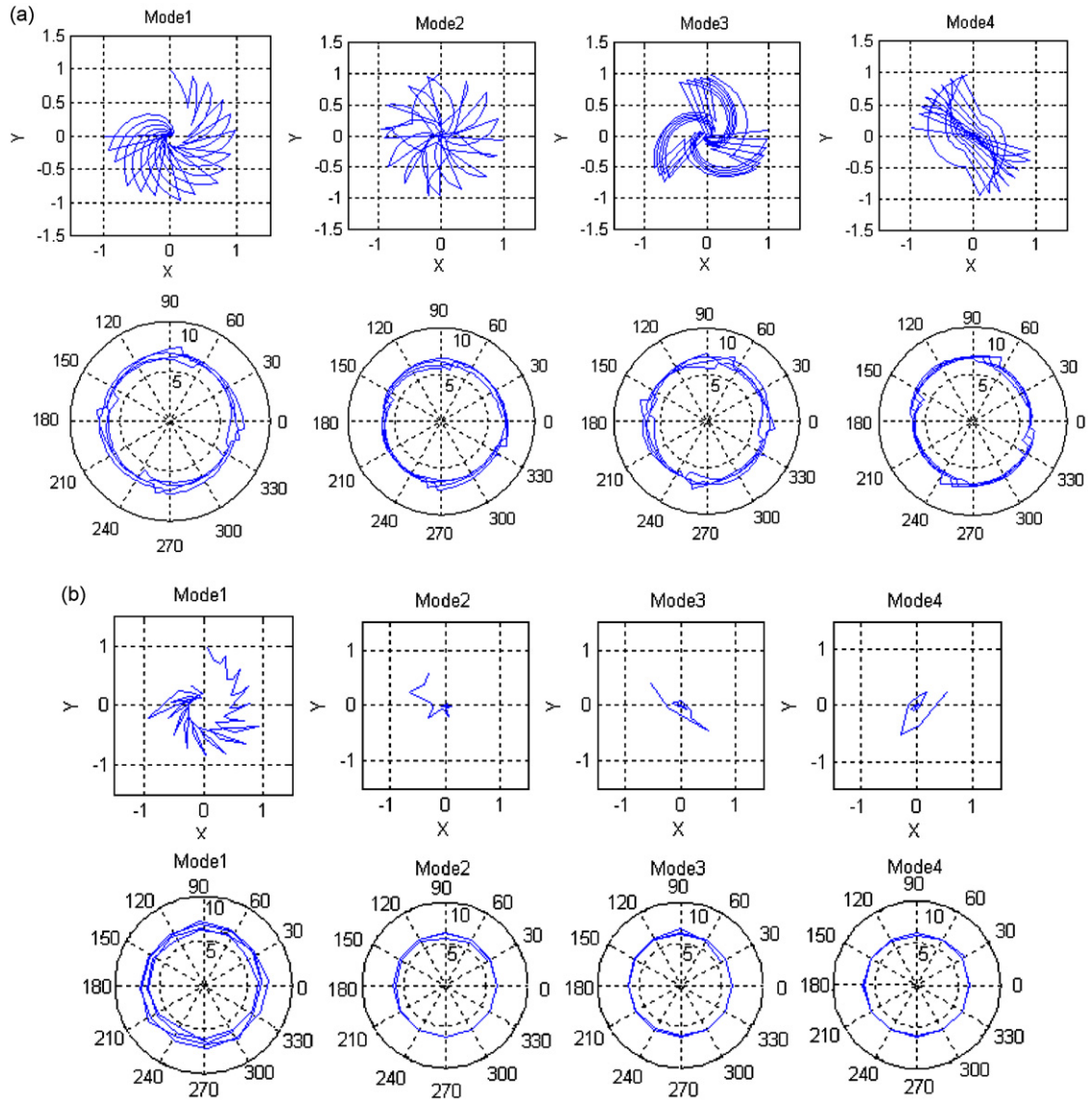

Fig. 13. Tool axis trajectory and hole profiles for the femur analogue for 32 element model of the reamer with the distributed force model: (a) regular, (b) irregular spacing.

Euler–Bernoulli beam elements with four degrees of freedom at each node. The application of loads on the reamer was considered in two scenarios: concentrated forces and distributed forces. In the latter, the cutting and rubbing forces were applied as uniform distributed forces on a variable engagement length which accounted for real engagement length of the reamers tapered with small angles. The governing equation of the process was based on a quasi-static model developed by Bayly [13]. Coefficients that were required in the model were found in a set of laboratory reaming experiments performed by Hojabr [7] on a femur analogue.

Cutting forces measured during the controlled reaming experiments were analysed to extract the required coefficients, which were then used to characterize the simulation of the reaming process in the femur analogue. Simulation results include reamer axis trajectories and the canals that result from the reaming process. Simulations depict non-cylindrical canals that result from low-frequency vibrations of common reamers with regular spacing. In order to reduce the vibrations during reaming of the femur, modifications in the reamer tooth spacing were investigated.

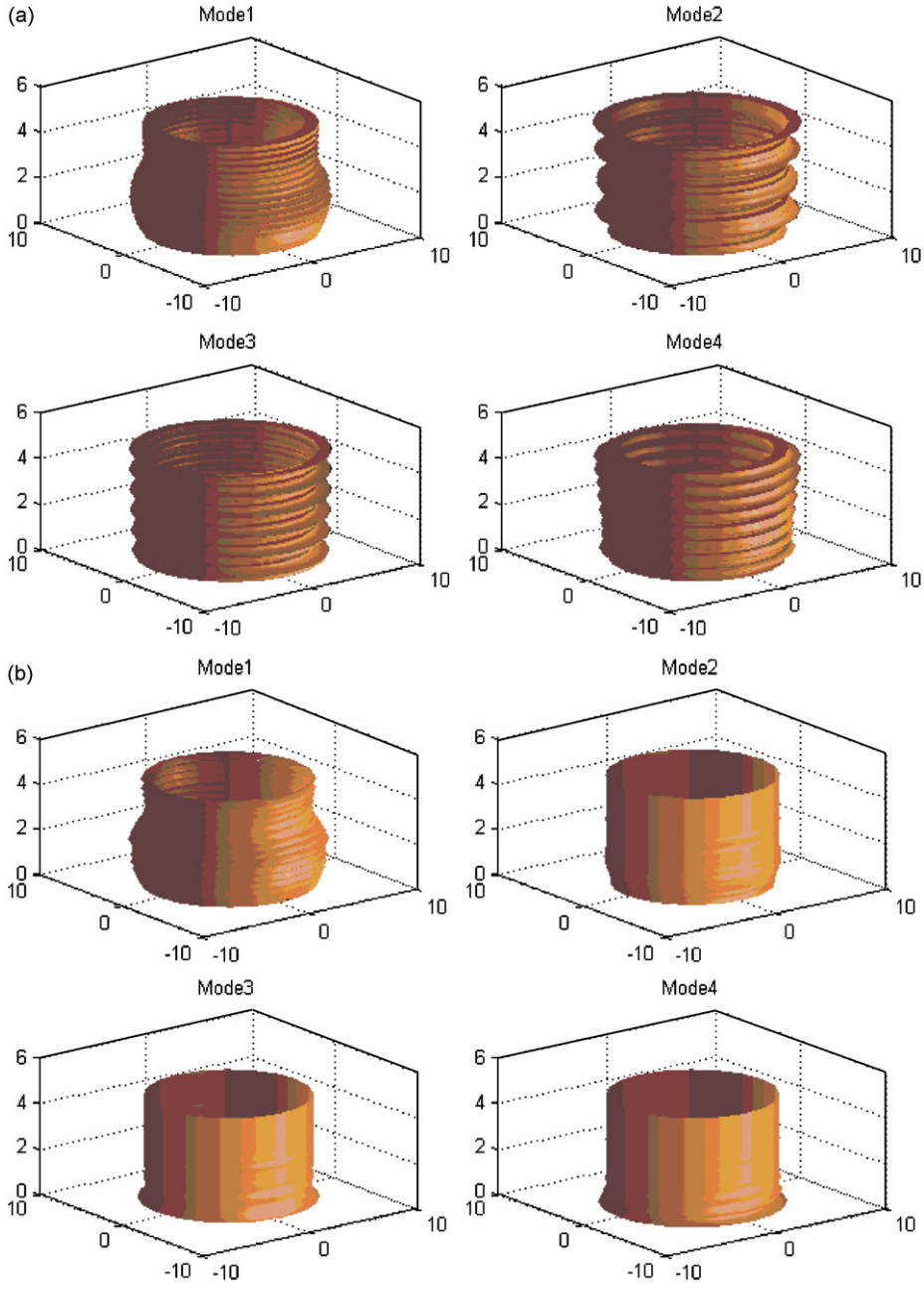

Fig. 14. Simulated 3D hole profiles for the femur analogue for 32 element model of the reamer with the distributed force model: (a) regular, (b) irregular spacing.

Modification of the reamer tooth spacing was been found to be an important parameter in reamer design and affects the vibration during reaming of the femur analogue. The optimum orientation for the teeth of a common six-flute reamer that yielded the maximum damping rate magnitude during the process and was the same as that found for reaming in aluminium by Towfighian et al. [6]. The optimum reamer led to the most stable reaming process with the highest damping rate resulting in a significant improvement in the canal quality. The rough texture of canals caused by using common reamers with regular tooth spacing has been made smoother by employing the reamer with the proposed optimum tooth spacing.

Some other parameters effective in reducing vibration during modelling of femur reaming were found to be decreasing the feed rate and increasing the bending stiffness of the reamer. Bending stiffness was higher for the reamers with a higher modulus of elasticity, shorter length and larger diameter. Therefore, where possible, using reamers with shorter length, larger diameters, and stiffer material is recommended in order to have lower vibrations and smoother canals after the process. In addition, for a specific reamer, lowering the advancement speed and increasing the rotation speed are recommended as doing so lowers the feed rates and results in more damped vibrations and, ultimately, canals with more cylindricality.

In summary, this new design for a reamer with irregular tooth spacing reduces vibrations and achieves more circularity and smoothness in the resulting canals, thus benefiting the subjects of orthopaedic surgery. This results in more rapid healing progress in patients with femur surgeries for intramedullary nailing which are among most widely practiced procedures in the treatment of long bone fractures. Another possible benefit of this research is lowering the risk of developing fat embolism syndrome during orthopaedic reaming operations by reducing vibratory excitation of the fracture fragments which is a potential factor affecting intravazation [2].

Acknowledgments

The authors would like to acknowledge the financial support of the Natural Science and Engineering Research Council of Canada (NSERC).

References

[1] R.J. Eveleigh, A review of biomedical studies of intramedullary nails, *Medical Engineering and Physics* 17 (5) (1995) 323–331.
[2] R.D. Peindl, M.E. Harrow, D.M. Banks, M.J. Bosse, J.F. Kellam, Assessment of reamer system mechanical loads as factors affecting intramedullary pressurization, *Proceedings of the 1997 ASME Bioengineering Conference*, Vol. 35, Sunriver, OR, 1997, pp. 247–248.
[3] R.D. Peindl, M.E. Harrow, D.M. Banks, M.J. Bosse, J.F. Kellam, Comparison of mechanical loads produced by current intramedullary reamer systems, *Journal of Orthopaedic Trauma* 12 (8) (1998) 531–539.
[4] B.H. Ziran, B. Klatt, M. Darowish, Un-reamed versus reamed to fit technique of tibial nailing in open fractures: evaluation of outcomes and cost analysis, *Proceedings of the Orthopaedic Trauma Association Annual Meeting Session VII*, San Antonio, TX, Paper no. 40, 2000.
[5] H.C. Pape, Kolk M. Aufm, T. Paffrath, G. Regel, J.A. Sturm, H. Tsherne, Primary intramedullary femur fixation in multiple trauma patients with associated lung contusion—a cause of posttraumatic ARDS, *Journal of Trauma* 34 (1993) 540–547.
[6] S. Towfighian, K. Behdinan, M. Papini, Z. Saghir, P. Zalzal, J. de Beer, Finite element modeling of low speed reaming vibrations with reamer geometry modifications, *Journal of Intelligent Manufacturing* 18 (6) (2007) 647–661.
[7] A. Hojabr, Experimental Characterization of the Pressure Buildup in the Intramedullary Canal During Orthopedic Reaming Using a Synthetic Bone Analogue, MASc Thesis, Ryerson University, Toronto, Canada, 2006.
[8] S.V. Kirsanov, Influence of reamer design on shape accuracy of machined hole, *Russian Engineering Research* 19 (11) (1999) 83–85.
[9] S.V. Kirsanov, Effect of reamer design on the faceting of machined holes, *Russian Engineering Research* 20 (4) (2000) 72–73.
[10] D. Dobrjanski, A. Hojabr, Z. Saghir, K. Behdinan, P. Zalzal, J. De Beer, M. Papini, Simulation of the pressure buildup in the intramedullary canal during orthopaedic procedures using a synthetic femur analogue, *Proceedings of the CSME Forum 2006* (*CD ROM*), Kananaskis, Alberta, Canada, May 2006.
[11] S.A. Tobias, *Machine Tool Vibration*, Wiley, New York, 1965.
[12] S. Smith, J. Tlusty, An overview of modeling and simulation of the mailing process, *Journal of Engineering for Industry* 113 (5) (1991) 169–175.
[13] P.V. Bayly, K.A. Young, S.D. Calvert, J.E. Halley, Analysis of tool oscillation and hole roundness error in a quasi-static model of reaming, *Journal of Manufacturing Science and Engineering* 123 (2001) 387–396.
[14] D.A. Stephenson, J.S. Agapiou, *Metal Cutting Theory and Practice*, CRC Press, Boca Raton, FL, Taylor & Francis, London, 2006.
[15] D.N. Dilley, Accuracy, Vibration, and Stability in Drilling and Reaming, DSc Dissertation, Washington University, St. Louis, 2003.
[16] S. Towfighian, Finite Element Modeling of Low Speed Reaming in the Application of Femoral Canal Preparation for Intramedullary Nailing, MASc Thesis, Ryerson University, Toronto, Canada, 2006.